UvA-DARE (Digital Academic Repository)

The effect of oxidation and resulfidation on (Ni/Co)MoS2 hydrodesulfurisation catalysts

Bremmer, G.M.; van Haandel, L.; Hensen, E.J.M.; Frenken, J.W.M.; Kooyman, P.J.

Link to publication

Citation for published version (APA):

The effect of oxidation and resulfidation on (Ni/Co)MoS$_2$ hydrodesulfurisation catalysts

G. Marien Bremmer[a,1], Lennart van Haandel[b,2], Emiel J.M. Hensen[b], Joost W.M. Frenken[c], Patricia J. Kooyman[d,*]

[a] Huygens-Kamerlingh Onnes Laboratory, Leiden University, Niels Bohrweg 2, 2333 CA, Leiden, the Netherlands
[b] Schuit Institute of Catalysis, Eindhoven University of Technology, Het Kranenveld 14, 5600 MB, Eindhoven, the Netherlands
[c] Advanced Research Center for Nanolithography, Science Park 110, 1098 XG, Amsterdam, the Netherlands
[d] Department of Chemical Engineering, University of Cape Town, Private Bag X3, Rondebosch, 7701, Cape Town, South Africa

ARTICLE INFO

ABSTRACT

The effect of a sequential oxidation and resulfidation treatment on γ-Al$_2$O$_3$ supported (Ni/Co)MoS$_2$ catalyst nanoparticles was investigated using (HR)TEM, XPS, and thiophene HDS catalytic performance experiments. Analysis of the HRTEM images revealed that, after initial sulfidation and oxidation, the resulfidation treatment restored the original slab length or increased it. The chemical composition of the samples, as determined by XPS, also slightly changed: the concentration of oxidic species increased, especially for the Ni promoter atoms. Comparing the catalytic HDS activity of the samples before and after the oxidation-resulfidation treatment showed that the catalysts were more than 20% more active after resulfidation. This increase in HDS activity is ascribed to a redistribution of the (Ni/Co)MoS$_2$ slabs during the second sulfidation treatment, indicating a size effect.

1. Introduction

Environmental legislation steers oil refineries towards producing transportation fuels that contain ever less sulfur contaminants [1]. Sulfur is typically removed using the catalytic hydro-desulfurisation (HDS) reaction, which exploits (Ni/Co)MoS$_2$ catalysts dispersed on γ-Al$_2$O$_3$ as support material [2,3]. MoS$_2$ catalysts consist of a single layer of molybdenum atoms sandwiched between two layers of sulfur, forming two-dimensional slab-like particles with a typical size of 2–3 nm [4,5]. Typical γ-Al$_2$O$_3$-supported MoS$_2$ catalysts contain both single catalyst slabs and stacks of multiple slabs. The catalytic performance in terms of activity and selectivity can be influenced by adding metal promoter atoms such as nickel or cobalt, yielding (Ni/Co)MoS$_2$ slabs [2,3,6]. As this catalytic system is used intensively, a lot of research effort to improve the catalyst is going on in both industry and academia.

Previous research indicated that experimentalists should be careful during preparation and handling of their MoS$_2$ catalyst samples as exposing the samples to air will change the particle size of the sulfide

entities [7]. Further investigations showed that oxidic species form on the edges of the (Ni/Co)MoS$_2$ catalyst slabs upon exposure to air [8]. These oxidic species seem to remain around a core of (Ni/Co)MoS$_2$ that still subsists, forming a ring-like barrier and thereby impeding further oxidation.

High-temperature resulfidation treatment of oxidized sulfidic catalysts has been reported to increase catalytic activity for CoMoS$_2$, but not for MoS$_2$ [9,10], whereas hardly any data are available for NiMoS$_2$ [11]. Only the study by Louwers et al. [11]. uses TEM to study the length of the sulfidic slabs, but even though they discuss the effects of exposure to air in detail they do not seem to take precautions to shield their sulfided catalysts from exposure to air between sulfidation and TEM analysis. Since the initial preparation of the catalyst involves the sulfidation of oxidic precursor species that finally form the (Ni/Co)MoS$_2$ slabs [12], it is expected that the newly formed oxidic species can be transformed back into sulfides. Two possible results of this approach could be that these sulfides would then aggregate into new (Ni/Co)MoS$_2$ crystallites, or combine with the still-existing (Ni/Co)MoS$_2$ cores causing these to grow back and resemble the situation as it was before

oxidation. The latter is what Louwers et al. conclude to take place [11].

To investigate this question, we prepared a series of NiMoS$_2$, CoMoS$_2$, and MoS$_2$ samples, supported on Al$_2$O$_3$. After initial sulfidation, we investigated the catalyst using high resolution transmission electron microscopy (HRTEM), X-ray photoelectron spectroscopy (XPS), and thiophene HDS catalytic performance experiments, then exposed the samples to a flow of artificial air (O$_2$/N$_2$, 20/80) for 24 h. Following this oxidation step, we subjected the samples to a second sulfidation treatment, identical to the initial sulfidation step. The samples were then investigated again using the aforementioned techniques. A second NiMoS$_2$ sample was also prepared using two consecutive sulfidation treatments, without an interim oxidation step, to compare the HDS activity data.

2. Experimental

2.1. Preparation of catalysts

The catalyst samples were prepared by incipient-wetness co-impregnation of Ketjen CK-300 γ-Al$_2$O$_3$ extrudates (S$_{BET}$ = 250 m^2/g, V$_{pore}$ = 0.66 ml/g), which were crushed and sieved to a 125–250 μm fraction prior to impregnation. Different solutions containing nickel(II) nitrate (Ni(NO$_3$)$_2$·6H$_2$O, Merck), cobalt(II) nitrate (Co(NO$_3$)$_2$·6H$_2$O, Merck), ammonium heptamolybdate ((NH$_4$)$_6$Mo$_7$O$_{24}$·4H$_2$O, Merck), and nitrilotriacetic acid (NTA) ((C$_2$H$_3$O$_2$)$_3$N, Merck) were prepared to obtain catalysts with 8 wt% Mo, as well as 1.5 wt% Ni or Co for the promoted catalysts. The molar ratio of NTA:Mo was 1.2:1. All catalyst precursors were dried at room temperature for 1 h, dried in static air at 100 °C overnight and finally calcined at 450 °C (heating rate 6 °C/min) in flowing air for 4 h. The catalyst precursors were sulfided at 350 °C (heating rate 6 °C/min) for 2 h in a flow of 60 ml/min STP H$_2$/H$_2$S 9:1 (Scott) at a total pressure of 1 bar.

To obtain samples denoted as oxidized, a portion of the freshly sulfided sample was placed in a glass tube, and a flow of O$_2$/N$_2$ (20/80, 150 mL/min) was set over the sample for 24 h at room temperature. After oxidation, the sample was re-sulfided via the same procedure used for the initial sulfidation.

After preparation, and in between each experimental step, the samples were collected, placed in a glovebox filled with N$_2$ (concentration of H$_2$O < 5 ppm, O$_2$ < 1 ppm), and sealed in glass vials until characterization.

2.2. TEM and XPS characterization of catalysts

TEM studies were carried out using a monochromated FEI Tecnai F20ST/STEM transmission electron microscope, operated at an accelerating voltage of 200 keV, in bright field TEM mode. Images were recorded using a Gatan Ultrascan CCD camera (4k × 4k).

The vials containing the samples were opened in an Ar-filled glovebox, after which the samples were crushed in n-hexane (Sigma-Aldrich, anhydrous, 95%) using a mortar and pestle, creating a suspension. A few drops of the suspension were placed on a Quantifoil® microgrid carbon film-covered mixed mesh Au TEM grid. After evaporation of the solvent at room temperature, the grid was placed in a

protective atmosphere transfer TEM specimen holder [13]. The sample compartment of the holder was closed and sealed by a Viton O-ring, and the holder was removed from the glovebox and transferred to the TEM for imaging. Once inserted in the TEM airlock, one three-minute pumping cycle was started while the holder was still closed, and the sample compartment of the holder was opened at the beginning of a second three-minute pumping cycle.

Samples were imaged after the initial sulfidation and after the oxidation-resulfidation treatment. Since the behavior of the samples upon mere oxidation was already thoroughly documented before [7,8], we did not characterize the oxidized samples. The resulting images were analyzed using ImageJ software. The length of each slab was measured by hand using standard drawing tools in the software. Around 500 individual slabs were measured for each sample. The mean slab length ($\bar{x}_c$) was obtained from the least-squares fit of a log-normal distribution to the slab length histogram, as is a common approach when modeling particle size distributions [14–17]. The average stacking degree (N) was calculated according to Eq. (1):

$$\bar{N} = \frac{\sum_i n_i N_i}{\sum_i n_i} \tag{1}$$

where N_i is the stacking number of a stack of MoS$_2$ (i.e., the number of MoS$_2$ platelets in the stack) and n_i is the amount of individual MoS$_2$ platelets counted for a given stacking number N_i.

The same samples were analyzed using a Kratos AXIS Ultra XP spectrometer, equipped with a monochromatic Al (Kα = 1486.6 eV) X-ray source and a delay-line detector (DLD). To prevent contact with air, samples were transferred from the glovebox to the XPS in a closed, homemade transfer holder under N$_2$ atmosphere. Survey scans were recorded at constant pass energy of 160 eV and region scans at 40 eV. The background pressure was 2 × 10^{-9} mbar.

XP spectra were fitted with CasaXPS (version 2.3.14) by a non-linear least-squares fitting algorithm using mixed Gaussian-Lorentzian (35/65) curves. Shirley background subtraction was applied and the energy was calibrated using the Al 2p peak at 74.6 eV as a reference. The Mo 3d spectrum was fitted with Mo^{4+} (MoS$_2$), Mo^{5+} (MoS$_x$O$_y$) and Mo^{6+} (MoO$_3$) contributions. The Ni 2p and Co 2p spectra were fitted with a sulfidic M^{2+} contribution and an oxidic M^{2+} contribution (NiO, CoO). The sulfidic contribution was assigned to Ni or Co sulfides, either dispersed on the edges of MoS$_2$ particles or present as bulk metal sulfides (Ni$_3$S$_2$, Co$_9$S$_8$). Lastly, the S^{2-} and bridged S$_2^{2-}$ anions, as well as sulfate anions (SO$_4^{2-}$), were taken into account for fitting the S 2p spectra. Binding energies of these components are listed in Table 1 and agree well with previously reported studies [18–20].

2.3. Catalytic activity

Atmospheric gas-phase thiophene HDS experiments were performed under differential conditions in a single-pass stainless steel flow reactor with an internal diameter of 4 mm. An amount of precisely weighed catalyst particles (approximately 25 mg for (Ni/Co)MoS$_2$; approximately 50 mg for MoS$_2$), diluted with 200 mg of SiC (250 μm), was sulfided in 60 mL/min H$_2$/H$_2$S(10%) at 350 °C for 2 h (6 °C/ min ramp) before the feed was switched to 4% (v/v) thiophene (Sigma − Aldrich)

Table 1

XPS binding energies of the various species possibly present in (Co/Ni)MoS$_2$, as used for the fitting procedure described in the text.

Species	Mo^{4+} (MoS$_2$)	Mo^{5+} (MoS$_x$O$_y$)	Mo^{6+} (MoO$_3$)	S^{2-} (MS$_x$)	S$_2^{2-}$ (MS$_x$)	S^{6+} (SO$_4^{2-}$)	Co^{2+} (CoS$_x$)[c]	Co^{2+} (CoO)[c]	Ni^{2+} (NiS$_x$)[c]	Ni^{2+} (NiO)[c]
BE (eV)[a]	229.0	231.0	232.6	161.7	163.3	168.8	778.7	781.7	853.9	856.5
ΔBE (eV)[b]	3.15	3.15	3.15	1.15	1.15	1.15	–	–	–	–

[a] Binding energy of the 3d$_{5/2}$ or 2p$_{3/2}$ peak. Uncertainty ± 0.2 eV.
[b] ΔBE(3d) = BE(3d$_{3/2}$) − BE(3d$_{5/2}$), ΔBE(2p) = BE(2p$_{1/2}$) − BE(2p$_{3/2}$).
[c] Only the 2p$_{3/2}$ peak was fitted for Co and Ni.

in H_2 at a flow rate of 100 mL/min (STP). Activity was determined using gas chromatography coupled with flame ionization detection (GC-FID). The reaction rate (r_{Thio}) normalized per mole of Mo was calculated according to Eq. (2):

$$r_{Thio} = \left(\frac{F_{Thio}}{m_{cat} w_{Mo}} \right) X \tag{2}$$

where F_{Thio} is the molar flow of thiophene ($mol_{Thio}\,h^{-1}$), m_{cat} the catalyst mass (g), w_{Mo} the fraction of molybdenum ($mol_{Mo}\,g_{cat}^{-1}$), and X the conversion. Initial conversion was high while steady-state activity was reached after approximately 13 h. The regular method to determine steady-state activity is by calculating the average activity of at least 4–5 h of steady-state data points. As some samples continued to show minor deactivation, even after 20 h of catalytic experiment, the activity data were fitted with a first-order exponential decay function and the horizontal asymptote was defined as the eventual steady-state activity of the catalyst (see Fig. S4).

3. Results & discussion

3.1. Imaging and slab length analysis

To determine the effect of the oxidation-resulfidation treatment on the slab size and dispersion of the different (Ni/Co)MoS_2 samples, they were characterized using TEM after the initial sulfidation treatment (the 'Zero' data) as well as after the resulfidation treatment (the 'Resulf' data). The length of the slabs was measured, and the resulting slab length distribution histograms are shown in Fig. 1. For NiMoS$_2$, the slab length distribution has shifted slightly towards higher slab lengths, indicating that the slabs have grown slightly longer after the second sulfidation treatment. This effect is almost negligible for MoS_2, and absent for CoMoS$_2$.

The intermediate oxidation step was shown to have a significant effect on the slab length distribution: 24 h of oxidation in ambient air
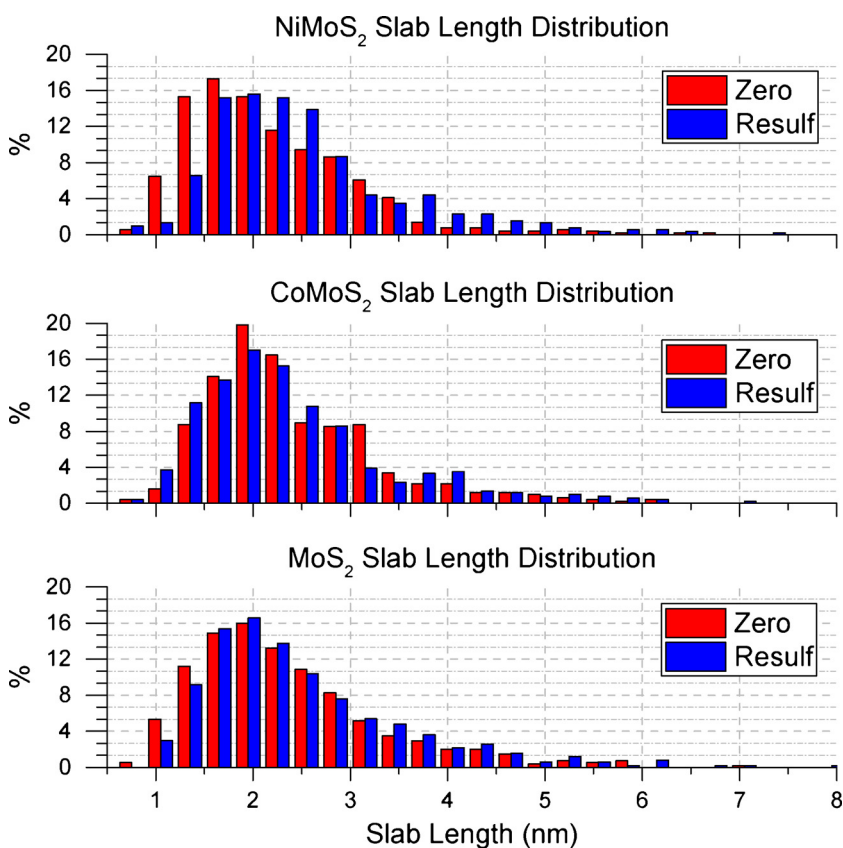
Table 2
Geometric mean slab length values ($\bar{x}_c$), geometric standard deviation (σ), and average stacking number of the samples.

		$\bar{x}_c$ (nm)	σ	Stacking
NiMoS$_2$	Zero	1.99 ± 0.03	0.39 ± 0.02	1.4
	Resulf	2.21 ± 0.03	0.31 ± 0.01	1.5
CoMoS$_2$	Zero	2.11 ± 0.02	0.37 ± 0.01	1.5
	Resulf	2.15 ± 0.03	0.34 ± 0.01	1.5
MoS$_2$	Zero	2.12 ± 0.03	0.34 ± 0.01	1.4
	Resulf	2.16 ± 0.04	0.31 ± 0.02	1.5

will shift the slab length distributions towards smaller slab lengths, while smaller slabs are disappearing completely [8]. As we now show that the slab length distribution of the resulfided sample resembles the starting situation reasonably well, we can conclude that the resulfidation treatment after oxidation causes the slabs to grow back to their original length or beyond.

To quantitatively compare the samples, the histograms were fitted with a log-normal distribution, and the geometric mean slab length ($\bar{x}_c$) and geometric standard deviation (σ) of each sample was calculated. In order to compare the stacking of the catalyst slabs, the average stacking numbers were calculated, showing the number of slabs per stack on average. The data are shown in Table 2. The fits of the histograms are shown in Fig. S1.

The mean slab length values confirm the trend visible in the histograms of Fig. 1. The NiMoS$_2$ sample shows an increase in mean slab length of approximately 10%. For MoS_2 and CoMoS$_2$, the mean slab length does not differ significantly from the freshly sulfided sample. The geometric standard deviation values are similar for all samples, and show that the slab length distribution of all resulfided samples has condensed into more narrow histograms. As for the average stacking, it remains practically the same for all samples between the different sulfidation treatments.

Fig. 1. Slab length distributions of (a) NiMoS$_2$, (b) CoMoS$_2$, and (c) MoS$_2$. Slab length distributions of both the freshly sulfided samples (Zero, red bars) as well as the oxidized and resulfided samples (Resulf, blue bars) are shown (For interpretation of the references to colour in this figure legend, the reader is referred to the web version of this article).
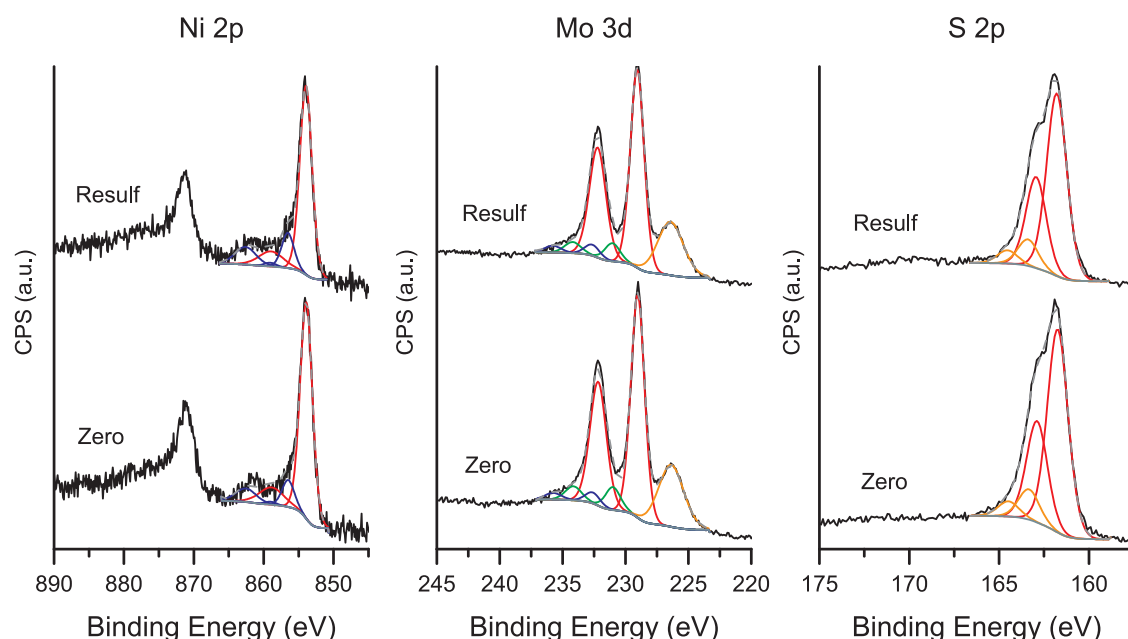
Fig. 2. XP spectra of NiMoS$_2$, showing the (a) Ni 2p, (b) Mo 3d, and (c) S 2p signals after initial sulfidation (Zero) and after the oxidation-resulfidation treatment (Resulf). The deconvolution consists of the following components: (a) Ni 2p: NiS$_x$, red; NiO$_x$, blue (both include satellites). (b) Mo 3d: Mo (IV), red; Mo (V), green; Mo (VI), blue; for S 2 s, orange. (c) S 2p: S^{2-}, red; S$_2^{2-}$, orange. In all graphs: background is light gray; fit is gray dashed; data is black (For interpretation of the references to colour in this figure legend, the reader is referred to the web version of this article).

3.2. Chemical state of the catalysts

The catalysts were analyzed using XPS directly after the initial sulfidation, as well as after the oxidation-resulfidation treatment. The resulting Ni 2p, Mo 3d, and S 2p spectra of the NiMoS$_2$ sample, including their deconvolution, are shown in Fig. 2. The spectra of CoMoS$_2$ and MoS$_2$ are shown in the Supporting Information (Figs. S2 and S3). The chemical composition of each sample was determined from the deconvolution of the spectra, giving the fractions of species that are in the sulfidic state, as shown in Fig. 3. The numerical data of Fig. 3 are shown in Table S1.

From Fig. 3 it is visible that after the initial sulfidation of the samples approximately 83% of Ni, 94% of Co, and 86% of Mo was present as sulfides, while the remainder of these species remained oxidic. The sulfur signal consisted solely of sulfidic species (S^{2-}, S$_2^{2-}$); no sulfur oxides were observed. Our previous study [8] showed that after 24 h of exposure to air approximately 15% of Mo, 6% of S, 39% of Ni and 24% of Co was oxidized compared with the freshly sulfided catalysts at t = 0. Oxidation of the Mo and S species occurred at approximately the same rates in both the promoted and unpromoted

samples. The promoted catalysts were most prone to oxidation as the Ni and Co atoms oxidized first. The oxidation of Co leveled off after 24 h of exposure to air, whereas Ni oxidation was an on-going process. After 1 month of exposure to air, all catalysts showed significant oxidation of all elements. Even sulfur, which oxidized more slowly than the other elements, was significantly oxidized after 1 month of exposure to air. The observed sequence of oxidation over time was: Ni/Co > Mo > S.

The effect of the oxidation-resulfidation treatment only had a small effect on the Mo and Co spectra of all three samples: the oxidic fraction of these components only slightly changed, between 0.4% and 2.1%. In the Ni spectra however, a significant increase in oxidic signal was observed after the oxidation-resulfidation treatment: the proportion of oxidized nickel increased by approximately 7%. This oxidative trend is in agreement with previous studies that showed the Ni/Co promoter atoms to oxidize more readily than Mo and S, and Ni to oxidize more deeply after 24 h in air [8]. As it was shown that after 24 h of oxidation all species had oxidized to a large extent (Ni 39%, Co 24%, Mo 15%, S 6%), it is clear that resulfidation occurs for all species.

It should be noted that during the initial sulfidation treatment, NTA has the effect of chelating the Ni/Co promoter atoms and delaying their
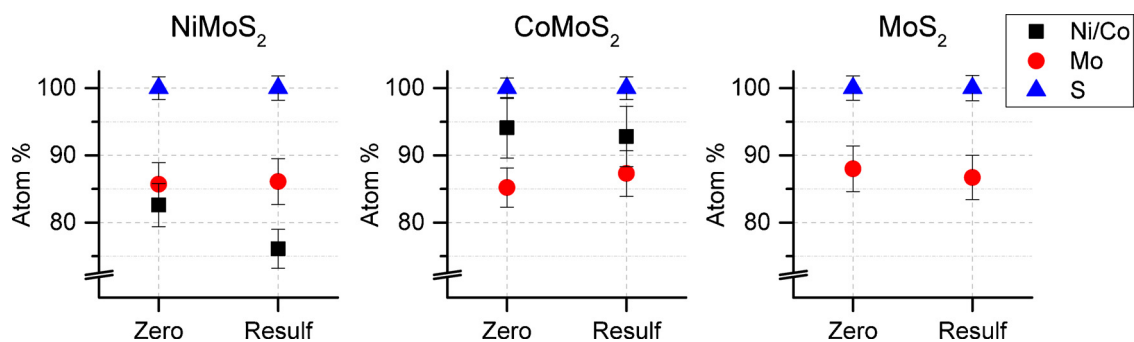
Fig. 3. Proportion of species present in the sulfidic state (in atom %, as determined by deconvolution of XP spectra). (a) NiMoS$_2$, (b) CoMoS$_2$, and (c) MoS$_2$, after initial sulfidation (Zero) and after the oxidation-resulfidation treatment (Resulf). The fraction of sulfided species was calculated from the contributions of MoS$_2$ (Mo^{4+}), sulfide anions (S^{2-} and S$_2^{2-}$) and sulfided Ni/Co (either as M-MoS$_2$ or as MS$_x$). Numerical data listed in Table S1. For each of the data points, the statistical error margins are indicated.

Table 3
Average steady-state catalytic activity data, normalized per mole of Mo, for gas-phase thiophene HDS.

		r_{Thio} ($mol_{Thio}\ mol_{Mo}^{-1}\ h^{-1}$) $\pm$ standard error of fit
NiMoS$_2$	Zero	37.0 ± 2.9
	Resulf	46.0 ± 2.1
	Doublesulf	44.2 ± 0.3
CoMoS$_2$	Zero	20.3 ± 4.8
	Resulf	28.2 ± 3.8
MoS$_2$	Zero	4.4 ± 0.1
	Resulf	5.4 ± 1.0

sulfidation to approximately 250 °C, while Mo starts sulfiding at approximately 150 °C already [21,22]. Since NTA decomposes mainly between 200 °C and 400 °C at 1 bar sulfidation pressure, the chelating agents will be removed during the first sulfidation treatment and the chelating effect will be absent in the second sulfidation treatment. The lack of chelating agents would cause all formed oxidic species (Ni, Co, Mo) to be sulfided at lower temperatures [21–23]. Surprisingly, the Ni promoter atoms, in contrast to Co and Mo, are not sulfided back to their initial degree of sulfidation, but a substantial proportion of the initially sulfided Ni promoter atoms remains oxidized after the resulfidation treatment: the initial sulfidation treatment left 17% of the Ni precursor species in oxidic form, which increased to 24% after the oxidation-resulfidation step.

3.3. Catalytic activity

The catalytic activity of the samples was determined in gas-phase thiophene HDS at atmospheric pressure. Steady-state activity was determined via a first-order exponential decay fit of the dataset, as shown in Fig. S4 and Table S2 in the Supporting Information. For each type of catalyst, activity data were obtained for two or three individual samples (e.g. Resulf 01 – 03; see Table S2). For comparison, an additional NiMoS$_2$ sample was treated with a second sulfidation treatment without the 24 h oxidation treatment in between. This sample is labeled 'Doublesulf'. Afterwards, the average steady-state activity was determined per group of samples. The resulting activity data are shown in Table 3.

Oxidation-resulfidation treatment clearly has a positive effect on the steady-state activity of the catalysts. All three samples show an increase of over 20%, while CoMoS$_2$ exhibits the largest activity increase with 39%. The Doublesulf NiMoS$_2$ sample showed a similar increase in HDS activity.

3.4. Discussion

The slab length analysis shows that the average (Ni/Co)MoS$_2$ slab length has increased after the oxidation-resulfidation treatment. The number of smaller slabs, below a size of 1.5 nm, has decreased, as is visible especially in the left shoulders of Fig. 1a and c. Still, the HDS activity of all catalyst samples has increased significantly. From previous research it is known that only the edges of the (Ni/Co)MoS$_2$ slabs are catalytically active [24,25], so from this perspective it is surprising that a catalyst sample that has larger particles and thus relatively less active edges available, is more active. The increase in activity might be caused by a redispersion process of the catalyst (and its promoter atoms) during the second heating step of the resulfidation treatment. The effect of the oxidation-resulfidation treatment might also be that the catalyst particles are now not completely sulfided and less well-crystallized, as was observed in previous experiments and which was suggested to cause more active sites for HDS [26].

Another potential explanation could be that there is a minimum size that a (Ni/Co)MoS$_2$ slab should have, above which it is catalytically

(more) active. Since the initially sulfided samples contain a larger proportion of smaller (< 1.5 nm) slabs, these slabs could fully oxidize during the oxidation treatment, and then redisperse and form larger, more active slabs during the second sulfidation treatment. This hypothesis is in line with the observation by Lauritsen et al. that MoS$_2$ nanostructures comprising less than 15 Mo edge atoms (21 atoms in total, particle size < ~1.6 nm) do not show the so-called electronic brim state that is believed to play an important role in HDS catalysis [27,28].

In view of this hypothesis, it might be favorable to tailor a (Ni/Co)MoS$_2$ catalyst as to have a narrower slab size distribution than is conventionally obtained via standard preparation methods, while the number of slabs smaller than ~1.6 nm is minimized. One way to achieve this is using a sequence of oxidation-resulfidation treatments.

4. Conclusions

(Ni/Co)MoS$_2$ slabs were prepared via an initial sulfidation step, and subsequently subjected to a 24 h oxidation and second sulfidation treatment. HRTEM showed that after oxidation and resulfidation the (Ni/Co)MoS$_2$ slabs were growing back to their original length or even slightly longer, while the width of the slab length distribution decreased. XPS showed that the oxidized molybdenum and sulfur returned completely to their freshly sulfided (pre-oxidation) states after resulfidation, whereas the cobalt and especially the nickel contained much larger proportions of oxidized species after the resulfidation. Moreover, the oxidation-resulfidation cycle resulted in an increase in HDS performance for gas-phase thiophene HDS, showing an activity increase of up to 40%. This increase in HDS activity seems to be due to both a redistribution of the (Ni/Co)MoS$_2$ slabs during the second sulfidation treatment (indicating a size effect with smaller slabs (< ~1.6 nm) being less active), as well as an increase in the amount of active sites due to incomplete sulfidation and crystallization of the slabs.

Declarations of interest

Acknowledgements

Appendix A. Supplementary data

Supplementary material related to this article can be found, in the online version, at doi:https://doi.org/10.1016/j.apcatb.2018.10.014.

References

[1] Environmental Protection Agency. Control of Air Pollution From Motor Vehicles: Tier 3 Motor Vehicle Emission and Fuel Standards Vol. 79 Final Rule, 2014.
[2] E.J.M. Hensen, V.H.J. de Beer, J.A.R. van Veen, R.A. van Santen, A refinement on the notion of type I and II (Co)MoS phases in hydrotreating catalysts, Catal. Lett. 84

(2002) 59–67, https://doi.org/10.1023/A:1021024617582.

[3] M. Egorova, R. Prins, The role of Ni and Co promoters in the simultaneous HDS of dibenzothiophene and HDN of amines over Mo/gamma-Al$_2$O$_3$ catalysts, J. Catal. 241 (2006) 162–172, https://doi.org/10.1016/j.jcat.2006.04.011.

[4] S. Eijsbouts, J. Heinerman, H. Elzerman, MoS$_2$ structures in high-activity hydrotreating catalysts, Appl. Catal. A Gen. 105 (1993) 53–68, https://doi.org/10.1016/0926-860X(93)85133-A.

[5] S. Eijsbouts, J. Heinerman, H. Elzerman, MoS$_2$ structures in high activity hydrotreating catalysts. II. Evolution of the active phase during the catalyst life cycle deactivation model, Appl. Catal. A Gen. 105 (1993) 69–82, https://doi.org/10.1016/0926-860X(93)85134-B.

[6] L.S. Byskov, J.K. Nørskov, B.S. Clausen, H. Topsøe, DFT calculations of unpromoted and promoted MoS$_2$-based hydrodesulfurization catalysts, J. Catal. 187 (1999) 109–122, https://doi.org/10.1006/jcat.1999.2598.

[7] P.J. Kooyman, J.A.R. van Veen, The detrimental effect of exposure to air on supported MoS$_2$, Catal. Today 130 (2008) 135–138, https://doi.org/10.1016/j.cattod.2007.07.019.

[8] G.M. Bremmer, L. van Haandel, E.J.M. Hensen, J.W.M. Frenken, P.J. Kooyman, Instability of NiMoS$_2$ and CoMoS$_2$ hydrodesulfurization catalysts at ambient conditions: a quasi in situ high-resolution transmission electron microscopy and x-ray photoelectron spectroscopy study, J. Phys. Chem. C 120 (2016) 19204–19211, https://doi.org/10.1021/acs.jpcc.6b06030.

[9] V.H.J. de Beer, C. Bevelander, T.H.M. van Sint Fiet, P.G.A.J. Werter, C.H. Amberg, The CoO-MoO$_3$-gamma-Al$_2$O$_3$ catalyst VI sulfur content analysis and hydrodesulfurization activtities, J. Catal. 43 (1976) 68–77.

[10] V.M. Browne, S.P.A. Louwers, R. Prins, Effect of passivation on the activity of sulfided Mo and Co-Mo hydrodesulfurization catalysts, Catal. Today 10 (1991) 345–352.

[11] S.P.A. Louwers, M.W.J. Crajé, A.M. van der Kraan, C. Geantet, R. Prins, Effect of passivation on the activity and structure of sulfided hydrotreating catalysts, J. Catal. 144 (1993) 579–596, https://doi.org/10.1016/j.cattod.2007.06.075.

[12] A.I. Dugulan, E.J.M. Hensen, J.A.R. van Veen, High-pressure sulfidation of a calcined CoMo/Al$_2$O$_3$ hydrodesulfurization catalyst, Catal. Today 130 (2008) 126–134, https://doi.org/10.1006/jcat.1993.1355.

[13] H. Zandbergen, P.J. Kooyman, A.D. van Langeveld, Electron microscopy, Proceedings of the 14th International Congress on Electron Microscopy Vol. II (1998) 491–492.

[14] A.K. Datye, Q. Xu, K.C. Kharas, J.M. McCarty, Particle size distributions in heterogeneous catalysts: what do they tell us about the sintering mechanism? Catal. Today 111 (2006) 59–67, https://doi.org/10.1016/j.cattod.2005.10.013.

[15] H.W. Haynes, Effect of particle size distribution on catalyst effectiveness, J. Catal. 79 (1983) 470–474.

[16] G. Renaud, R. Lazzari, C. Revenant, A. Barbier, M. Noblet, O. Ulrich, F. Leroy, J. Jupille, Y. Borensztein, C.R. Henry, J.P. Deville, F. Scheurer, J. Mane-Mane, O. Fruchart, Real-time monitoring of growing nanoparticles, Science 300 (2003) 1416–1419, https://doi.org/10.1126/science.1082146.

[17] C.G. Granqvist, R.A. Buhrman, Size distributions for supported metal catalysts: coalescence growth versus Ostwald ripening, J. Catal. 42 (1976) 477–479, https://doi.org/10.1016/0021-9517(76)90125-1.

[18] T. Weber, J.C. Muijsers, J. Van Wolput, C.P.J. Verhagen, J.W. Niemantsverdriet, Basic reaction steps in the sulfidation of crystalline MoO$_3$ to MoS$_2$, as studied by x-ray photoelectron and infrared emission spectroscopy, J. Phys. Chem. 100 (1996) 14144–14150, https://doi.org/10.1021/jp961204y.

[19] I. Alstrup, I. Chorkendorff, R. Candia, B.S. Clausen, H. Topsøe, A combined x-ray photoelectron and Mössbauer emission spectroscopy study of the state of cobalt in sulfided, supported, and unsupported Co-Mo catalysts, J. Catal. 77 (1982) 397–409, https://doi.org/10.1016/0021-9517(82)90181-6.

[20] A.D. Gandubert, C. Legens, D. Guillaume, S. Rebours, E. Payen, X-ray photoelectron spectroscopy surface quantification of sulfided CoMoP catalysts – relation between activity and promoted sites – part I: influence of the Co/Mo ratio, Oil Gas Sci. Technol. Rev. IFP 62 (2007) 79–89, https://doi.org/10.2516/ogst:2007007.

[21] L. Coulier, V.H.J. de Beer, J.A.R. van Veen, J.W. Niemantsverdriet, Correlation between hydrodesulfurization activity and order of Ni and Mo sulfidation in planar silica-supported NiMo catalysts: the influence of chelating agents, J. Catal. 197 (2001) 26–33, https://doi.org/10.1006/jcat.2000.3068.

[22] L. van Haandel, G.M. Bremmer, E.J.M. Hensen, T. Weber, The effect of organic additives and phosphoric acid on sulfidation and activity of (Co)Mo/Al$_2$O$_3$ hydrodesulfurization catalysts, J. Catal. 351 (2017) 95–106, https://doi.org/10.1016/j.jcat.2017.04.012.

[23] L. van Haandel, G.M. Bremmer, P.J. Kooyman, J.A.R. van Veen, T. Weber, E.J.M. Hensen, Structure–activity correlations in hydrodesulfurization reactions over Ni-promoted Mo$_X$W$_{(1-X)}$S$_2$/Al$_2$O$_3$ catalysts, ACS Catal. (2015) 7276–7287, https://doi.org/10.1021/acscatal.5b01806.

[24] M. Salmeron, G.A. Somorjai, A. Wold, R. Chianelli, K.S. Liang, The adsorption and binding of thiophene, butene and H$_2$S on the basal plane of MoS$_2$ single crystals, Chem. Phys. Lett. 90 (1982) 105–107, https://doi.org/10.1016/0009-2614(82)83620-8.

[25] J.G. Kushmerick, P.S. Weiss, Mobile promoters on anisotropic catalysts: nickel on MoS$_2$, J. Phys. Chem. B 102 (1998) 10094–10097, https://doi.org/10.1021/jp982752.

[26] P.J. Kooyman, J.G. Buglass, H.R. Reinhoudt, A.D. van Langeveld, E.J.M. Hensen, H. Zandbergen, J.A.R. van Veen, Quasi in situ sequential sulfidation of CoMo/Al$_2$O$_3$ studied using high-resolution electron microscopy, J. Phys. Chem. B 106 (2002) 11795–11799, https://doi.org/10.1021/jp0256701.

[27] J.V. Lauritsen, J. Kibsgaard, S. Helveg, H. Topsøe, B.S. Clausen, E. Lægsgaard, F. Besenbacher, Size-dependent structure of MoS2 nanocrystals, Nature Nanotechnol. 2 (2007) 53–58, https://doi.org/10.1038/nnano.2006.171.

[28] F. Besenbacher, M. Brorson, B.S. Clausen, S. Helveg, B. Hinnemann, J. Kibsgaard, J.V. Lauritsen, P.G. Moses, J.K. Nørskov, H. Topsøe, S.T.M. Recent, DFT and HAADF-STEM studies of sulfide-based hydrotreating catalysts: insight into mechanistic, structural and particle size effects, Catal. Today 130 (2008) 86–96, https://doi.org/10.1016/j.cattod.2007.08.009.